# SEISMIC PERFORMANCE AND FINANCIAL RISK OF MASONRY HOUSE

**J. K. Bothara[1], J. B. Mander[2], R. P. Dhakal[3], R. K. Khare[4], M. M. Maniyar[5]**

## ABSTRACT

Seismic behaviour of typical unreinforced masonry (URM) brick houses, that were common in early last century in New Zealand and still common in many developing countries, is experimentally investigated at University of Canterbury, New Zealand in this research. A one half-scale model URM house is constructed and tested under earthquake ground motions on a shaking table. The model structure with aspect ratio of 1.5:1 in plan was initially tested in the longitudinal direction for several earthquakes with peak ground acceleration (PGA) up to 0.5g. Toppling of end gables (above the eaves line) and minor to moderate cracking around window and door piers was observed in this phase. The structure was then rotated 90º and tested in the transverse (short) direction for ground motions with PGA up to 0.8g. Partial out-of-plane failure of the face loaded walls in the second storey and global rocking of the model was observed in this phase. A finite element analysis and a mechanism analysis are conducted to assess the dynamic properties and lateral strength of the model house. Seismic fragility function of URM houses is developed based on the experimental results. Damping at different phases of the response is estimated using an amplitude dependent equivalent viscous damping model. Financial risk of similar URM houses is then estimated in term of expected annual loss (EAL) following a probabilistic financial risk assessment framework. Risks posed by different levels of damage and by earthquakes of different frequencies are then examined.

**KEYWORDS:** Unreinforced masonry (URM), seismic performance, fragility, expected annual loss (EAL), hazard survival probability.

## 1. Introduction

Dynamic tests of unreinforced masonry (URM) buildings and wall components have been conducted in different parts of the world in order to investigate rehabilitation requirements of such building. Tomazevic (1987) tested dynamically a one-seventh scaled four-storey unreinforced brick masonry model building. His model possessed a reinforced concrete rigid floor diaphragm and masonry piers from floor to ceiling height. Since all the damage was observed in the first storey, he recommended a storey mechanism model for the analysis of such buildings. He also tested three 1:4 scale two-storey model houses constructed in brick laid in cement, lime and sand mortar with timber floors representing old historic houses (Tomazevic 1996). The models were constructed with and without roof ties to investigate and compare the effect of these ties on the seismic behaviour of such buildings. He concluded that the behaviour of URM houses depended on the rigidity of the floor diaphragm and the connection between the diaphragm and the walls. Qumaruddin and Chandra (1991) conducted shaking table tests of small scale URM building models. They reported that the walls supporting floor/roof suffer more damage if the shaking is normal to them unless the strength of in-plane walls is mobilised through diaphragm action.

[1] *Seismic Engineer, Beca Carter Consultants, Wellington, NZ*
[2] Zachry *Professor, Department of Civil Engineering, Texas A&M University, College Station, Tx 77843 3136, Texas, USA*
[3] *Senior Lecturer, Department of Civil Engineering, University of Canterbury, Private Bag 4800, Christchurch, NZ*
[4] *Professor, Department of Civil Engineering, S.G. S. Institute of Technology & Science, Indore - 452003, India*
[5] *Research Scholar, Department of Civil Engineering, S.G. S. Institute of Technology & Science, Indore - 452003, India*

Response of an instrumented two-story URM shear wall building with flexible diaphragms has been reported previously by Tena-Colunga and Abrams [1992]. This triggered a whole series of experimental investigation on URM houses with flexible floor diaphragms. Calvi and Pavese (1995) conducted full scale tests on a two-storey brick masonry physical model with flexible floor diaphragm to explore dynamic parameters and failure mechanisms in URM buildings. Costley and Abrams (1996) reported tests of two 3/8 scale models constructed in brick with cement, lime and sand mortar with flexible floor and roof to explore simplified methods for evaluation and rehabilitation of URM buildings. Benedetti and Pezzoli (1996) conducted a comprehensive study to investigate the behaviour of URM buildings before and after seismic intervention. They reported testing of 24 half-scale URM buildings models constructed of brick or stone in lean mortar and flexible floor and roof representing existing masonry buildings. Recently, Peralta et al (2002) investigated seismic performance of rehabilitated floor and roof diaphragms in pre-1950s unreinforced masonry buildings, and Yi et al (2006 a,b) conducted experimental and analytical investigations on the seismic behaviour of a two-storey URM building.

In addition to the above mentioned dynamic testing of 3-dimensional models, dynamic tests have been conducted on URM components as well to investigate their seismic performance. Magenes and Calvi (1995) conducted dynamic tests on eight URM walls to scrutinize the influencing parameters such as mortar strength and aspect ratio on in-plane failure modes and compared the results with quasi static tests conducted on similar specimens. They found good correlation between dynamic and quasi-static test results in terms of failure mechanism and interaction of fundamental parameters. Doherty (2000) and Simsir et al (2002) have reported dynamic testing of scaled URM masonry walls conducted to investigate their out-of plane behaviour. They concluded that the out-of-plane collapse of URM walls is primarily associated with excessive displacement rather than attainment of static out-of-plane strength of the walls.

Increasing interest in the last few decades in masonry construction has resulted in research and prescription of seismic vulnerability assessment methodologies for URM buildings. For this purpose, visual assessment methods are prescribed by several sources such as: FEMA154 (1988), Sobaih (1999) and NSET (2000). Detailed assessment methods are given by Arya (1992), NZSEE (1995), NZSEE (2006), FEMA356 (2000) and Tomazevic (1999). Magenes (2000) has given a more comprehensive description of an assessment procedure of URM buildings based on the preceding works by Magenes and Calvi (1999). The study conducted by Moon et al (2006) has led to recommendations for seismic evaluation and retrofit of low-rise URM structures.

For out-of-plane vulnerability assessment of URM walls, Priestley (1985) proposed a velocity-based approach founded on equal-energy principle considering the energy balance of the responding walls and reserve capacity of rocking walls. However, in this method the energy demand is very sensitive to the selection of elastic natural frequency. Lately, displacement-based approach has been proposed by various researchers including Doherty (2000), Doherty et al (2002), Griffith et al (2003) and Griffith and Magenes (2003). They have proposed a tri-linear static force-displacement relationship for seismic vulnerability assessment of out-of-plane walls. In particular, Griffith et al (2003) predicted collapse by using “appropriate” stiffness and elastic response spectra and, in contrast to Priestley (1985), argued that the initial stiffness (thereby the initial period) is not crucial in determining the occurrence of collapse. De Felice and Giannini (2000, 2001) studied out-of-plane resistance of masonry walls based on simple collapse mechanisms and conducted numerical analysis taking into account the connection between the longitudinal and transverse walls. ATC40 (1996) proposed a new displacement based seismic evaluation methodology based on the Capacity Spectrum Method for reinforced concrete buildings. The method utilizes the acceleration-displacement response spectra (Mahanay et. al., 1993) as demand curve and pushover curve as the capacity curve. The method has been used by Costley and Abrams (1996) to predict in-plane capacity of unreinforced brick masonry model buildings.

Present work seeks to estimate financial loss through investigation of the dynamic performance of URM houses. In this context, a half scale brick masonry house with a flexible floor and roof was dynamically tested on shaking table. It investigates deficiencies in URM houses, and their effect on

the overall seismic performance. Furthermore, it focuses on the development of an analytical method to generate fragility functions to predict the extent of damage in such houses at various levels of ground shaking based on the experimental observations. Fragility curves thus drawn are used to estimate financial loss. The authors are aware of some studies investigating fragility of URM structures (Craig et al 2002, Park et al 2002, Towashiraporn et al 2002) but none have extended the fragility functions to seismic loss assessment. An earthquake–recurrence relationship is defined to transform earthquake intensity to annual frequency. A loss ratio, which is the ratio of the cost necessary to restore the full functionality of the structure to the replacement cost, is then assigned to each damage state observed experimentally. Expected annual loss (EAL) is calculated using the extension of the Pacific Earthquake Engineering Research (PEER) Centre's triple integral formulation (Krawinkler and Miranda, 2004), which has been extended by Dhakal and Mander (2005) to a quadruple integral equation. Limitations of the study and sensitivity to various parameters are reported. Comments useful to owners and insurers of the buildings are made from an insurance point of view.

## 2. Experimental Investigation

A two-storey half-scale URM model house was constructed and tested under earthquake ground motions on a shaking table. The one-room per floor house was constructed with clay brick masonry laid with cement-lime-sand mortar. The model house had a conventional timber floor and timber frame roof clad with clay tiles. The layout of openings, door and windows were sized and located to be representative of a range of a typical construction practice. The chosen model represents a generic non-engineered masonry house. Two examples of prototype in Nepal and New Zealand are given in Bothara (2004). Due to the shaking table limitation a length scale of half (1:2) was adopted for this study. Thus, twin wythe walls were replicated in the model as a single wythe. The model was constructed with the same material as the idealised prototype. By adopting constant acceleration similitude, constant stress and strain similitude are also achieved. This led to the following scale factors: force scale, $S_F = ¼$; frequency scale, $S_f = 1.414$; time and velocity scale $S_t = S_v = 0.707$; and mass density scale $S_\rho = 2$. The model structure with aspect ratio of 1.5:1 in plan was initially tested in the longitudinal direction against several earthquakes with PGA up to 0.5g. The structure was then rotated 90º and tested in the transverse (short) direction against ground motions with PGA in excess of 0.5g.

For the mass similitude, live loads were ignored. Additional masses of 120 kg, 1.97 tonne and 2.1 tonne were required at the gable walls, floor and eaves level, respectively. Out of the 120kg of additional mass required, only 36 kg could be attached to each gable wall due to space constraint and the rest were added at the eaves level during the longitudinal testing. Additional masses of 2.05 tonne and 2.09 tonne were added at the floor level and eaves level, respectively. When testing in the transverse direction, the gable walls were not loaded with additional loads and this load was added to the eaves level load. To load the front and back walls, additional masses were fixed to the floor joists and roof ties. To load the side walls for stress simulation, platforms were constructed, one end of which was rigidly tied to the transverse walls and other end rested on the sliding joints supported on floor joists or roof ties.

### 2.1 Model Construction

The foot print of the 3.2m high model was 2.88x1.92m as shown in Figure 1. In constructing the model house, recycled full size *wire cut* bricks typical of early 1930s known as the "seventy series" were used. Based on customary building practices in early last century a mortar mix of 1:1:6 (cement: lime: sand) was adopted. Coarse river sand consisting up to 3mm particle size was used for the mortar with hydrated lime and ordinary Portland cement as binder. *Rimu*, a native New Zealand wood, was used for rafters and flooring material. For the rest of the woodwork, *Pinus Radiata* was used. A standard procedure was adopted in constructing the model house. During the

construction of the model house, comprehensive tests were conducted to track mechanical properties of the masonry. Average values of mechanical properties are presented in Table 1.

Doors and windows were constructed of 30x50mm timber section with a bearing of 75mm on wall. The floor was constructed of 10mm thick and 85mm wide *Rimu* tongue and groove flooring nailed to 35x125mm timber joists. The joists were nailed to 35x50mm wooden wall plates laid on the front and back walls. The wall plates just rested on wall without any mechanical anchorage with the wall. The end joists were nailed to the side walls and structurally isolated from floor planks to isolate these side walls from the front and back walls. A tiled roof was laid on a 33-degree pitched timber frame, and the roof accommodated around 2 tonne of additional mass. Roof purlins were simply seated on the gable walls without any nailing. To observe the relative performance of different roofing practices, all roof tiles on one pitch and alternate roof tiles on the other pitch were tied down with binding wires to the purlins when tested in the longitudinal direction. However, when tested in the transverse direction, half of the tiles on one side were untied and rest were alternatively tied down; and on the other slope all the tiles were tied down.

### 2.2 Experimental Procedure

A total of 61 and 41 channels of instruments were employed to collect data during the dynamic excitations of the model in longitudinal and transverse directions, respectively. Accelerometers and linear potentiometers were the principal instruments used. The potentiometers were employed to measure crack openings at pre-determined locations, shear deformations of the piers, and sliding between floor/roof and the walls. In order to measure the relative displacement between floor/roof and face loaded walls, potentiometers were attached at the floor and roof levels along the central line of the side solid wall during longitudinal shakings and the front wall during transverse shakings. Moreover, the in-plane shear deformation of the piers was measured by attaching potentiometers diagonally across piers 1-4 in the front wall (see Figure 2) during longitudinal shakings and across piers 11-14 (see Figure 2) during transverse shakings. Similarly, one accelerometer was attached to the base slab to track input acceleration history, and accelerometers were attached to the middle of the four walls at the floor and roof levels to measure movement of the model (at different locations) in the direction of shaking. Data was collected via a purpose-built data acquisition system operating at 400Hz and 1000Hz during the longitudinal and transverse shakings, respectively.

The testing program was basically divided into two parts: i) identification of dynamic characteristics; and ii) investigation of the behaviour of the model building in strong shaking. For identification of dynamic properties, white-noise shaking tests were conducted. To investigate building response to strong shaking, it was subjected to frequency-scaled earthquake ground motions. Sequence of the shaking table tests performed in the longitudinal and transverse directions is presented in Table 2 and Table 3, respectively.

### 2.3 Experimental Results

#### 2.3.1 Longitudinal Direction Shaking

Cracks developed during different stages of the longitudinal shaking are shown in Figure 2. Figure 3 presents the photographs of the damage suffered by the model during this shaking. It should be noted that no instability of any part of the model was observed (excluding gable walls) during the longitudinal shaking tests. A vertical crack was observed in the mortar joint of the rowlock brick just above the front wall door after the Taft (0.2g) excitation as shown in Figure 2. During the Taft (0.3g) excitation, one of the gable walls cracked and started to rock at the eaves level, just below the additional load fixing level of the end wall. A residual displacement of 3 mm was observed at the top of the gable wall at the end of this excitation.

During the RA01168 (0.5g) excitation the other gable wall also cracked at its base (seen in Figure 2 and Figure 3b) and started to rock. A few more cracks were observed just below the top of the gable walls and in the bottom and top of the front wall piers (shown in Figure 3c). A compression crack below Pier #4 at the wall corner and compression edge failure at the bottom of the rocking gable walls and its base were also observed during subsequent shakings.

As can be seen in Figure 2, a vertical flexural crack developed between the 1st and 2nd storey windows in one side during the EL40NSC excitation. As shown in Figures 3d and 3e, the cracks developed just below and above the pier in earlier shaking articulated into stair-stepped crack pattern. A horizontal crack was also observed just above the floor wall plate in the front wall. From the maximum displacements measured during different shakings, the weighted displacements are calculated at the seismic centre of mass of the model, which are listed in Table 4 for both longitudinal and transverse shaking directions.

### 2.3.2 Transverse Direction Shaking

Figure 4 presents the cracks developed, and Figure 5 presents the photographs of damage suffered by the model during different excitations in the transverse direction. It should be noted that no instability of any part of the model (front and back walls suffered partial instability) was observed during the transverse shaking tests. As can be observed in Figure 4, most of the cracks concentrated in the out-of-plane wall of the second-storey whereas the side window wall (in-plane) suffered extensive damage in both the first and second storeys. Cracking was also observed in the solid side wall. Most of cracks developed during earlier excitations in the longitudinal direction widened and extended during the stronger excitations of this phase of testing.

Small vertical cracks were observed above the second storey windows of the front wall after the Taft (0.2g) excitation. During the Taft (0.3g) excitation, a few new cracks opened at the bottom of the side walls. During the EL40NSC excitation, extensive cracks developed in the out-of-plane walls as seen in Figure 4. Vertical cracks developed along the line of jambs of the second storey openings in the front wall, practically isolating the wall from the in-plane walls. Similar vertical or stair-step cracks developed above the long window of the back wall (see Figure 5d). Once the severe cracking of the model started, dislocation of lintel timber pieces and permanent distortion of the opening frames were also observed.

During the RA01168 (0.7g) excitation, cracks that had previously developed widened, and some new cracks developed. A stair-step crack was observed just above the first storey window and in the pier of the second storey wall (see Figure 5a) in the front wall. The front wall rocked about a horizontal crack along the mortar bed joint observed at the floor level during this shaking. During the SYLM949 excitation, extensive cracks developed in both the in-plane and out-of-plane walls. As can be seen in Figures 4 and 5b, more stair-step cracks were observed in the spandrel beam of the front wall and along the mortar joint bed in the back wall. Also can be clearly seen in Figure 4 is a full length horizontal crack developed along the bottom of the gable wall of the side window wall. Similar crack was also observed at the floor level of the side window wall. The vertical cracks in spandrel beam and below first storey window of the side window wall effectively divided the wall in two significant tall piers. During the Nahanni excitation, the cracks further widened, however, no new cracks were observed.

No significant relative displacement between the floor and the supporting walls was observed. This contradicts the observed behaviour in past earthquakes where relative movement between floor structure and walls was reported (Bruneau 1994, NSET 1999). The first reason could be the model was quite stable until the end of the testing without much distress in the first storey. The other reason could be: there was around 2 tonne of mass on the floor structure that mobilised friction between the floor wall plate and the supporting walls, which would not exist in this magnitude in real structure.

It is noteworthy that few of the roof tiles which were not tied down with the roof structure, scattered badly and few of them slid off the roof slope during the RA01168 (0.5g) excitation. As shown in Figure 5f, these tiles slid off catastrophically during the RA01168 (0.7g) excitation and other big excitations. It is interesting to note the tile sliding started from the roof edge. However, no tiles tied down with the timber frame moved much and slid off the roof. Note that the model survived higher acceleration than expected for real URM masonry buildings in the field mainly because no local failure started that would lead to instability, and the building behaved like a box. This can be attributed to good connection between the orthogonal walls at the junctions, good connection between floor/roof and walls, diaphragm effect, better construction/material quality and good foundation which are usually not available in most real buildings.

### 2.3.3 Frequency domain observations

Dynamic properties of the model were computed from the response acceleration time histories collected during the shaking table test. To avoid the effect of input amplitude, transfer functions for individual channels were calculated by normalising Fast Fourier Transfer (FFT) of each response channel by FFT of the input motion (in this case input acceleration at the base slab level). Intrinsic damping was calculated from Transfer function plots applying half-power bandwidth method (Chopra, 1995). The mode shapes were calculated by taking ratio of peaks in the transfer function for different degrees of freedom at any particular natural frequency. Because the constant of proportionality is the same for all degrees of freedom for any particular mode, the ratio of peaks in the transfer functions for the different degrees of freedom at that natural frequency are equal to the ratio of the mode shapes for that mode (Bracci et. al., 1992). The dynamic stiffness of the model was estimated using the relation $K=4\pi^2Mf^2$ where only the first mode was considered. In this relation 'M' is the seismic mass of the building and 'f' is the measured frequency.

### 2.3.4 Inferred hysteretic damping

Total equivalent viscous damping in a dynamic inelastic system is a sum of hysteretic damping, radiation damping associated with the rocking and intrinsic damping due to internal interactions within the system. From the *displacement versus acceleration* hysteretic loops, the hysteretic damping can be estimated using $\varsigma_{eq} = \frac{1}{4\pi}\frac{E_D}{E_{so}}$ (Chopra, 1995), in which $E_D$ = total area enclosed by the hysteretic loop and $E_{so}$ = strain energy imposed on the system.

From the displacement-acceleration plots of different sets of channels, hysteretic loops for the same time intervals were developed. For these loops, hysteretic damping was estimated and then weighted for their tributary mass. Similarly, the corresponding displacement of the seismic mass centre was estimated for these loops. The equivalent hysteretic damping after each series of shaking (i.e. calculated corresponding to the recorded hysteresis loops) is listed in Table 4.

## 3. Analytical Study

An analytical investigation of the model was conducted through finite element simulation and simple rational calculations. The calculations based on a plastic mechanism analysis were performed to estimate the strength of the model. The dynamic structural characteristics of the models were assessed through finite element simulation and a static condensation technique. Note that although it was intended to construct a flexible diaphragm, the resulting floor was rigid because of the tongue & groove flooring, high strength/stiffness of the diaphragm, scale effect, connection between wall and floor etc. Hence, a rigid diaphragm system was assumed whenever needed in analytical modelling.

### 3.1 Finite Element Analysis

A linear elastic finite element model using four node shell elements for walls was developed in SAP2000 (CSI 2002). Masonry was assumed to be isotropic (Dhanasekar et al 1982). The floor joists of the model were comprised of beam elements which were pinned at the ends. The floor boards were modelled as discrete plane elements isolated from the walls. Roof rafters and ties were discretised as beam elements and ties were pinned at the ends. The dynamic modulus of elasticity was assumed as 390MPa based on the average measured crushing strength of masonry (Mengi & McNiven, 1986) rather than the measured static modulus of 6100MPa. It is because dynamic modulus of elasticity is much lower than the static one (Mengi & McNiven, 1986). This point is also proved by measured frequencies. If the static modulus of elasticity had been used to calculate the frequency in the longitudinal direction, the predicted frequency of the model would have been in the range of 40Hz, far more than the measured values.

Static analysis of the model suggested flexural cracking to be the dominant mode of damage. In longitudinal shakings, analysis showed that the cracks would develop at the top and bottom of the front wall piers. In transverse shakings, flexural cracks were expected to develop in the front wall above the second storey windows corners. With increasing levels of lateral load, the bottom of the in-plane walls showed development of tensile cracks. Estimated base shear capacity at which the cracks would develop during longitudinal and transverse shakings and the corresponding deflections are shown in Table 5.

Table 6 presents the frequencies computed from dynamic analysis using the linear finite element model. Out-of-plane behaviour of the walls normal to the shaking was observed as the most dominant mode of vibration. For comparison, the frequency and mode shapes of the model were also estimated assuming a 2-degree of freedom system using a static condensation technique assuming undamped vibration (Chopra, 1995). For calculation of frequency, mass is assumed lumped at floor and roof level only. In full-scale URM houses, these types of floors hardly contribute 10-20% of the building mass and such houses are better represented by distributed mass system. However, in the tested model, additional mass required for stress simulation was fixed to the floor and roof which was around 50% of the model mass, thereby justifying the lumped mass assumption. The finite element analysis in SAP2000 also lumps the mass at certain level even if the system is distributed one. The comparison of dynamic properties from the finite element analysis and from the static condensation technique is shown in Table 6.

### 3.2 Mechanism Analysis

Base shear capacity is the capacity of the building at which the building gets to the onset of plastic behaviour. Thus the base shear capacity/coefficient of the model is calculated in this study from mechanism analysis as prescribed by NZSEE guidelines. Force based approach (Paulay and Priestley, 1992) is used to determine the in-plane strength of the model. Overturning moments were considered for strength estimation of the wall piers. For the estimation of base shear coefficients at cracking, a storey failure mechanism of the model structure (pier action of the wall) was assumed. To assess the strength of the model, plastic analysis was conducted. The front wall (with door and window openings) was found to be dominated by rocking whereas the back wall to be shear dominated in longitudinal shaking.

For the front wall, it was predicted that cracking would initiate at a base shear of 24kN and a rocking mechanism would develop at 32kN. The model was expected to develop a mechanism at a base shear coefficient of 0.7 (54kN). The side walls were predicted to develop tensile crack at their bases in transverse shaking at a base shear coefficient of 0.36 (28kN). After that, it was obvious that these walls would globally rock about their base. The model was expected to rock at a global base shear coefficient of 0.55 (42kN).

### 3.3 Comparison of Experimental and Analytical Results

As predicted analytically, the front wall ground floor piers rocked when the model was shaken in the longitudinal direction. However, the rocking surfaces manifested in stair-step cracking as well in few piers rather than just at the bottom or top. As predicted, the back wall turned out to be much stronger than the front wall and did not suffer any damage in general. The experimental pier cracking strength in longitudinal shaking was 23% higher than the analytical prediction. However, at the first cracking, 0.69mm displacement was observed as compared to 0.18mm at eaves level calculated analytically using static modulus of elasticity. This shows that the model was much softer than estimated using the static modulus of elasticity.

In the transverse direction, the predicted cracking strength was found to be 17% higher than the experimentally observed strength. However, once the model started global rocking, the predicted base shear coefficient was found closer to the observed one. Some cracks observed during the experiments were found in reasonably good agreement with the predictions of static analysis. Differences between the experimental and analytical predictions of elastic frequency and deflection were considerable if estimated using the static elastic of modulus. For example, the experimental fundamental frequency in the longitudinal direction observed before cracking was 13.7Hz as against 33.1Hz and 38Hz estimated respectively from SAP2000 and static condensation using the static modulus of elasticity. On the other hand, using the value of dynamic modulus of elasticity estimated using the crushing strength of masonry (Mengi & McNiven, 1986) predicted a reasonable frequency, but not the deflections. Other sources of error in the estimation of frequency and displacements could be the uncertainty associated with the load transfer mechanism, flange effect and in the assumed material properties.

## 4. Development of response and fragility functions

In order to conduct seismic risk analysis, probabilistic relationships between the seismic intensity of the earthquakes and the maximum response (called the response function) and between the maximum response and a damage measure (called a fragility function) need to be established. If the earthquake intensity is expressed in terms of the PGA (which is not uncommon in seismic risk assessment methodologies), the results of the different series of the shaking table tests will give a series of PGA vs. maximum response points. As the number of data points is limited by the number of tests and the maximum response during the later tests will be influenced by the prior shakings, an alternate method to predict the PGA vs. the maximum response is implemented here. As derived by Pekcan et al (1999), the relationship between the earthquake intensity (PGA) and the maximum displacement of a structure can be expressed as higher of:

$$PGA = 2\pi\sqrt{\frac{C_c \Delta_{\mathrm{Pr}\,ototype}}{g}} B_\varsigma, \qquad PGA = 0.4 C_C B_\zeta \tag{1}$$

where $C_c$ = base shear capacity as determined from the finite element analysis (0.7 for longitudinal direction and 0.55 for transverse direction); $\Delta_{\mathrm{Pr}\,ototype}$ = maximum displacement of the seismic mass center of the prototype and $B_\varsigma$ is a damping related reduction factor. According to Martinez (2002), this factor is given by:

$$B_\varsigma = \sqrt{\frac{0.05 + \varsigma_{eff}}{0.1}} \tag{2}$$

where $\varsigma_{eff}$ = effective viscous damping estimated from displacement-damping relationship as follows (Pekcan et al 1999):

$$\varsigma_{eff} = 0.05 + \frac{2}{\pi}\eta\left(1 - \frac{\Delta_y}{\Delta_{\max}}\right) \tag{3}$$

where $\eta$ = efficiency factor taken here as 0.5, $\Delta_y$ = displacement at the first crack (from the test results, it is 0.7 mm and 1.05 mm for the longitudinal and transverse directions, respectively) and $\Delta_{max}$ = maximum displacement at the seismic mass centre. The effective viscous damping predicted by Equation (3) includes the inherent damping in the system (assumed as 5%) and the hysteretic damping estimated as $2\eta/\pi(1-\Delta_y/\Delta_{max})$. For verification, the equivalent hysteretic damping in the longitudinal and transverse directions predicted by this expression is plotted in Figure 6 together with the hysteretic damping estimated from the experimental results. It can be seen in the figure that Equation (3) reasonably captures the variation of damping with the displacement amplitude. Now using this damping and the base shear coefficient determined earlier, a deterministic median response function can be established using Equation (1). The incorporation of uncertainties in the response function is described later.

To generate fragility functions, numbers from one to five that refer to increasing level of damage are used, as defined in Table 7. Note that this is a common form of damage classification format as adopted by HAZUS (1999). Based on post-earthquake utility and life-safety considerations, the drift ratios observed during the tests at the onset of different level of damage are summarised in Table 8. Note that the damage states vs. drift relationships are assumed to be deterministic in this study and due to lack of data, uncertainties in these fragility relationships (which are inevitable) are not considered. Next, combining the response and fragility functions, the median PGA corresponding to the boundaries of different damage states can be calculated using Equations (1)-(3), which are also presented in Table 8.

In dynamic analysis, the resulting variability in the response function results entirely from the randomness of the input motion; i.e. if two different records are scaled to the same PGA, the maximum response would still be different. As the computational modeling is conducted using crisp input data, the epistemic uncertainty is not accounted for. However, the structural resistance both in terms of strength and displacement capacity is also inherently variable. To encompass the randomness of seismic demand along with the inherent randomness of the structural capacity and the uncertainty due to inexactness of the computational modeling, an integrated approach as suggested by Kennedy et al. (1980) is used in this study. If the randomness and uncertainties are assumed to be distributed normally or log-normally (which is a common assumption in probabilistic seismic risk assessment), the composite value of the lognormal coefficient of variation (i.e. dispersion factor) can be expressed as:

$$\beta_{C/D} = \sqrt{\beta_C^2 + \beta_D^2 + \beta_U^2} \tag{4}$$

in which $\beta_C$ = coefficient of variation for the capacity which arises as a result of the randomness of the material properties that affect strength; assumed to be $\beta_C = 0.2$ in this study; and $\beta_D$ = coefficient of variation for the seismic demand which arises from record-to-record randomness in the earthquake ground motion suite and found to be $\beta_D = 0.52$ in this study; and $\beta_U$ = lognormal dispersion parameter for modelling uncertainty found to be approximately $\beta_U = 0.2$ based on results given in Table 4. Using the aforementioned values of $\beta_C$, $\beta_D$ and $\beta_U$, Equation (4) gives $\beta_{C/D} = 0.6$.

As indicated earlier, the PGAs shown in Table 8 are the median ($50^{th}$ percentile) values. Using these median values and the lognormal coefficient of variation = 0.6 (as calculated above), the probability of the damage during an earthquake (of given PGA) being within a given state can be shown graphically through vulnerability curves as in Figure 7. Two vertical lines are drawn at 0.4g and 0.72g to represent respectively the design basis earthquake (DBE) and the maximum considered earthquake (MCE) at Wellington, following the seismic hazard reported in the New Zealand loading standard (NZS1170.5 2004). The intersection of these vertical lines with these damage probability curves gives the probability of different damage states for the corresponding seismic hazard. Figure 7 shows that some 30% of the URM houses will suffer irreparable damage (DS4) or collapse (DS5) in a DBE, while up to 70% may suffer damage that would be either slight or

repairable (DS1-DS3). However if an MCE was to strike, then some 65% of such houses might suffer irreparable damage or collapse with remaining 35% suffering minor or repairable damage.

## 5. Financial Seismic Risk Assessment Framework

Communicating seismic risk to decision makers is an important aspect of performance based earthquake engineering (PBEE). One such communication tool is Expected Annual Loss (EAL) which can be expressed in a dollar value. EAL incorporates the entire range of seismic scenarios, return rate, and expected damage into a median dollar loss. Though there are many methods of quantifying financial risk, EAL is especially useful to decision makers for cost-benefit analysis of design alternatives for new structures or seismic retrofit alternatives for existing structures. Moreover, EAL can easily be accounted for by including into operating budgets.

In addition to the response and fragility functions, an EAL assessment process also requires a seismic hazard occurrence relationship (correlating earthquake intensity with its annual frequency of occurrence) and a loss model (correlating damage with probable loss). When these four relationships are combined using a quadruple integral shown below, seismic risk can be quantified in terms of EAL (Dhakal and Mander 2005).

$$EAL = \int_0^1 \int_0^1 \int_0^1 \int_0^1 L_R . \left| dP[L_R \middle| DM] \right| . \left| dP[DM \middle| EDP] \right| . \left| dP[EDP \middle| IM] \right| . \left| df_a[IM] \right| \quad (5)$$

In Equation (5), IM = intensity measure; $f_a$[IM] = annual frequency of an earthquake of a given intensity IM; EDP = engineering demand parameter; DM = damage measure; $L_R$ = loss ratio (i.e. decision variable); P[A|B] = shortened form of P[A ≥ a | *B*=b]; and dP[A|B] = derivative of the conditional probability P[A|B] with respect to A. In this study, rather than using Equation (5) analytically, the integrations are conducted numerically. In fact, the integration of the response function (i.e. IM/EDP relationship; i.e. P[EDP|IM]) and the fragility function (i.e. EDP/DM relationship; i.e. P[DM|EDP]) has implicitly been performed deterministically (for median values) in Table 8 and using the combined uncertainty predicted by Equation (4), probabilistic vulnerability curves (i.e. IM vs. DM curves; i.e. P[DM|IM]) have been generated in Figure 7. A hazard recurrence relationship (between $f_a$ and IM; i.e. $f_a$[IM]) and a loss model (between DM and $L_R$; i.e. P[$L_R$|DM]) need to be established to complete the remainder of the EAL assessment process, which is explained below.

## 6. Assessment of Hazard Survival Probability

### 6.1 Earthquake Recurrence Relationship

Based on historical earthquake data, relationship between the peak ground acceleration (PGA) of earthquakes (denoted as $a_g$) with their annual frequency of occurrence ($f_a$) has been established as:

$$a_g = \frac{a_g^{DBE}}{(475 f_a)^q} \quad (6)$$

where $a_g^{DBE}$ is the PGA of the DBE (10% probability of occurrence in 50 years) and $q$ is an empirical constant found to be equal to 0.33 for seismic hazard in New Zealand (NZS1170.5 2004).

### 6.2 Hazard Survival Curves

Vulnerability curves of Figure 7 can now be re-plotted by changing the horizontal axis from IM to $f_a$ using the earthquake recurrence relationship established earlier. Such curves are called hazard-survival curves and they show the annual probability of the (seismic hazard induced) damage exceeding different limit states. Figure 8 shows the hazard survival curves for a typical URM house, which also give the probability of damage in such URM masonry houses falling within a limit state

when an earthquake of a given annual frequency strikes. Two vertical lines representing the annual probabilities of DBE ($f_a$ ~ 0.002) and MCE ($f_a$ ~ 0.0004) are also shown in the plots for reference. The intersections of any vertical line through a value of $f_a$ with the hazard survival curves give the probability of these damage states not being exceeded in earthquakes of that annual probability of occurrence. Thus obtained damage state survival probabilities in earthquakes of different frequencies are shown in Table 9 for a typical URM house of the tested type. Similarly, Table 10 shows the probabilities of being in a given damage state (confidence interval) for a typical URM house. For example, the second row in Table 9 means that if an earthquake of annual frequency of 0.01 (i.e. return period of 100 years) strikes, the probability of DS1 not being exceeded in an URM house of the tested category is 74%; and the corresponding probabilities for damage state DS2, DS3 and DS4 are 84%, 92% and 96% respectively. Similarly, the second row of Table 10 indicates that in a 100 year return period earthquake, there is a 74% chance that the damage state of URM houses will be DS1, 10% chance that the damage will be in the range of DS2, 8% chance that the damage will be in DS3, 4% chance the damage will be in DS4 and 4% chance of DS5.

## 7. Financial Implication of Earthquakes

### 7.1 Loss Model

To quantify financial loss, a loss model must be established to relate damage measure (DM) to a dollar value. In this study, the financial implication of each damage state is represented by a *loss ratio* ($L_R$), which is the ratio of the cost necessary to restore the structure to full working order to the replacement cost. Deciding the cost implication of each damage state is a subjective process and the accuracy of the decided value will depend largely on the amount of time devoted to researching repair costs and their variation by extent of damage, location of building, etc.

The assumed values and the likely range of loss ratios for different damage states are shown in Table 11. As no damage or repair is expected in the elastic state DS1, no financial loss is incurred and the loss ratio for DS1 is therefore zero. Loss ratio for DS2 is likely to fall between 0.05 and 0.15 to account for minor repairs due to slight but tolerable damage, and $L_R$ = 0.1 is assumed for DS2. The loss ratio for DS3 may vary from 0.2 to 0.4 for repairing the incurred moderate damage to restore functionality, and a representative value of 0.3 is adopted in the present analysis. "Irreparable damage" under DS4 demands complete replacement as repair may be uneconomic; hence the loss ratio of 1 is used here. Similarly for DS5, which is complete failure/collapse the value of loss ratio is 1. It has been shown (Dhakal and Mander, 2005) that the financial risk is sensitive to the values of loss ratios, especially $L_R$ for DS2 and DS3. Hence, good judgement should be applied in deciding these values. Also, the $L_R$ values for DS1 (no damage), DS4 (irreparable damage) and DS5 (collapse) are certain and obvious, there is likely to be uncertainties in the $L_R$ values for DS2 (slight damage) and DS3 (moderate damage). This study has not attempted to quantify these uncertainties, which are hence not taken into account here.

### 7.2 Probable Loss in an Earthquake

Using the assigned loss ratios, the contribution of different damage states to the financial loss can be estimated. Table 12 lists the probable financial loss (as fraction of the total replacement cost) due to different damage states when earthquakes with annual frequencies of 0.1, 0.01, 0.001, 0.0001, and 0.00001 strike. The values in Table 12 are the products of the probability of being in a given damage state in earthquakes of different annual frequencies (obtained from corresponding Table 10) and the consequence; i.e. the loss ratio for the corresponding damage state (obtained from Table 11). Graphical version of Table 12 is shown in Figure 9, which exhibits the contributions of different damage states and the total probable loss in the form of bar charts.

As expected, DS1 does not incur any financial loss as it does not need any repair. Similarly, the financial loss incurred by earthquakes of 0.1 or higher annual frequency is also negligible as such frequent events do not incur any damage requiring repair or replacement (DS2 or higher damage

category). As confidence intervals of higher damage states are multiplied by larger values of $L_R$, the higher damage-states contribute more to the probable loss although the likelihood of the earthquake-induced damage falling into these severer categories is not high.

The total financial loss due to earthquakes of a given probability shown in the last column of Table 12 is the sum of the contributions of the five damage states. The loss hazard curve shown in Figure 10 plots the probable losses of a typical URM house against their annual frequency of exceedance. These curves also give information on what would be the financial loss if an earthquake of a given annual frequency strikes once. As expected, the larger and rarer the event the greater the financial loss. Conversely for frequent but low intensity events, the single-event loss is small.

Two vertical lines corresponding to DBE and MCE are also shown in the figures. It is evident from Figure 10 that URM houses are likely to lose about 37% and 70% of its value due to damage incurred by a DBE and an MCE, respectively. A loss of 11% is possible even by the earthquakes of 0.01 annual frequency (i.e. return period of 100 years). Similarly, 50% loss is probable in an earthquake of 1000 years return period.

### 7.3 Calculation of Expected Annual Loss (EAL)

The total expected annual loss can be calculated using Equation (5) by integrating the loss ratio ($L_R$) over all possible annual frequencies of the seismic hazard; i.e. between 0 and 1. This general equation in continuous form can be expressed as:

$$\mathrm{EAL} = \int_0^1 L_R \, df_a \tag{7}$$

In discrete form, the expected annual loss (EAL) can be calculated as:

$$\mathrm{EAL} = \sum_{all\, l_{r,i}} \left( \frac{l_{r,i} + l_{r,i+1}}{2} \right) \left( f_a[L_R = l_{r,i}] - f_a[L_R = l_{r,i+1}] \right) \tag{8}$$

in which $f_a[L_R=l_r]$ is the annual frequency of the loss ratio being equal to a given value $l_r$ which can be obtained from the loss hazard curve (Figure 10). Table 13 shows the annual loss of URM houses. First, the probable loss due to earthquakes of annual probability within a range is calculated which is the area subtended by the loss hazard curve (Figure 10) between two points on the x-axis. Then the losses contributed by the earthquakes with different ranges of probability are added together to obtain the total expected annual loss (EAL). It can be noted that the annual probability is plotted in logarithmic scale in Figure 10, and the absolute value of the interval between any two points on the x-axis decreases by an order of ten towards the left. Accordingly, the absolute value of the area covered is also decreasing rapidly in that direction (i.e. direction of decreasing probability) in spite of a higher value of the loss ratio.

As can be observed from Table 13, the EAL of typical URM houses is $8772 for a $1 million house (i.e. 0.88%). Note that this model overestimates the EAL by over-emphasising the contribution of frequent events which are not likely to cause any significant damage requiring repair. The error can be compensated by truncating the data below a certain threshold. This threshold is found by locating the IM at which there will be no damage, say with 90% confidence. As shown in Figures 7 and 8, earthquakes with PGA $\approx$ 0.16 (annual probability of 0.032 and return period of approximately 31 years) will have 90% probability of remaining in DS1; i.e. not inducing any damage to URM houses. Hence, the contribution to EAL of earthquakes below this threshold can be excluded for objectivity. In this example, EAL is found to be about 45% lower after truncating the contribution of earthquakes below this threshold.

## 8. Discussion: Implications to Owners and Insurers

The outcome of this analysis can provide useful information for deciding insurance strategies, but the applicability of any quantitative outcome from this study is limited to the category of URM

houses which are covered by the model used in this study. Any major alterations in the properties of the houses may lead to qualitatively similar but quantitatively different results. Although the tested model was designed to represent URM houses in NZ (Bothara 2004), the population of masonry houses in a country is difficult to be represented by a single type. In New Zealand, masonry houses are not built anymore and there are few existing old masonry houses, and they somewhat resemble with the tested house. On the other hand, masonry houses in Nepal (and India) vary widely. Obviously, the outcome of the study is not quantitatively extendable to URM houses of significantly different features. Nevertheless, the financial risk assessment procedure followed here is applicable to all structural types and by inputting appropriate fragility and response functions, the expected annual loss for any other type of URM houses can be derived.

Vertical ordinate of the loss hazard curve (Figure 10) gives the probable loss (due to structural damage) of a house due to an earthquake of a given annual frequency of occurrence. Hence, these curves also represent the financial risk (excluding content loss) to the owners of such houses. Evidently, smaller and more frequent events will cause only a small loss to owners of such URM houses. Consequently, owners may be prepared to bear the risk of these frequent earthquakes by themselves. When moderate earthquakes (with a return period of 100 years) strike, the probable loss is only about 11% of the building value. On the other hand, a rarer and stronger earthquake may often incur a loss of 50% or more, thereby rendering the repair uneconomical and necessitating replacement. House owners would obviously be more inclined to pass the risk affiliated to such disastrous consequences to insurers.

Note that the risk (defined as the product of probability and consequence in general terms) encompasses all possible hazards. In other words, the integration of the loss hazard curve (Figure 10) represents total risk due to structural damage of a URM house. As EAL is the area subtended by the loss hazard curve, it therefore represents an insurer's risk and is directly related to an annual insurance premium for a building if the consequences of all levels of seismic hazards are to be covered. The contribution of earthquakes of different frequency ranges to the total EAL is also graphically illustrated in Figure 11. Looking at the trend in Table 13 and Figure 11, it is apparent that the more frequent and smaller events that contribute more to the total financial risk, and the large earthquakes lead to much smaller risks due mainly to their very small annual frequency of occurrence (long return period). For example, among the total EAL of the URM house ($8772 per $1 million replacement value) investigated in this study, 60% corresponds to the risk posed by frequent but modest size earthquakes with an annual frequency in the range between 0.01 and 0.1 (i.e. return periods between 10 and 100 years).

Although the risk posed by large and rare events is small, the loss to owners would be untenable if these large events occur. That is why most insurance policies are targeted to cover the rarer and bigger hazards. In contrast, the smaller and more frequent events will cause a small loss to the individual owners but a significant collective risk to the insurers. If these frequent hazards are excluded from the insurance policy, the EAL and consequently the annual insurance premium will reduce significantly. From an insurance point-of-view, the risk of these smaller and more frequent events should ideally be carried by the owner. This can be achieved by setting an appropriate deductible to the insurance policy, which is a minimum loss which has to be borne by the owner in every event. For example, if the overhead costs of the insurer is overlooked and the premiums are assumed to reflect directly the risks, an insurance policy with a $1,000 deductible on a URM house worth $1 million implicitly means (see Figure 10) that the owner is completely bearing the consequence of earthquakes of up to approximately 100 years return period.

## 9. Conclusions and Recommendations

Seismic performance of a typical 2-storey URM house subjected to various ground motions in longitudinal as well as transverse directions has been experimentally investigated in this study. Damage was limited to toppling of gable walls and some cracking around window and door piers during the longitudinal shakings. During the shakings in transverse direction, the second-story face-

loaded walls rocked and tended to fail in the out-of-plane direction. The acquired experimental data were processed to generate fragility functions of such URM houses. A finite element analysis has also been performed to assess the strength and dynamic structural characteristics of the experimental model. An amplitude dependent equivalent viscous damping model, which has been verified by the experimental results, was used to estimate the relationship between the earthquake intensity and the maximum response of the model. Thus developed response and fragility functions were combined with a code-specified hazard recurrence model and a loss model to calculate the expected annual loss (EAL) of typical URM houses by using a generalised probabilistic financial risk assessment methodology.

Based on the experimental investigations and the financial risk analysis conducted in this study, the following conclusions can be drawn:

1. Gable walls and roofing clay tiles, if present, are the most vulnerable part of an URM house. These could be life threatening even if the house, as a whole, survives an intense shaking. Toppling gable walls and sliding off the roofing tiles could be inhibited by securing them back to the roof structure.

2. Out-of plane failure of the walls is the major cause behind high damage to URM houses in shaking. It can be significantly suppressed by increasing the bond strength between orthogonal walls, providing rigid diaphragm and reducing their horizontal and vertical span.

3. Rocking is the most preferred mode of failure in walls of URM houses because it leads to a stable non-linear response.

4. In-plane damage is mostly concentrated in zones of high shear stress, notably the bottom storey. Out-of plane damage occurs mostly in zones of high response acceleration and starts from the top storey.

5. If a DBE strikes in Wellington, some 30% of the URM houses might suffer irreparable damage or collapse. However, for an MCE event, some 65% of the URM houses might suffer irreparable damage or may collapse probably leading to loss of life. It is also found that the URM houses are likely to incur about 37% and 70% loss in a DBE (10% in 50 years event) and an MCE (2% in 50 years event), respectively. The EAL of a typical URM house in Wellington is found to be in the order of $8772 per $1million asset value (i.e. 0.88%). Note that these predictions are made by using earthquakes recorded in firm soil in California and are hence valid only if these records are representative of earthquake risk and hazard of Wellington.

6. Although the consequence of very large earthquakes might be disastrous, they pose relatively small financial risk due to their very low probability of occurrence. On the other hand, smaller earthquakes may only cause repairable minor-moderate damage to structures, but these earthquakes pose a big risk as they are likely to strike more often. Calculations showed that earthquakes with a return period between 10 and 100 years would contribute approximately 60% to the annual financial risk in case of URM houses.

7. A low-premium insurance policy with an appropriate deductible amount can be set, so that the risk posed by frequent and moderate earthquakes (which has minor consequence) is born by the owners, and disastrous consequence of rare but large earthquakes (which pose relatively smaller risk) is covered by the insurer.

While this study has given interesting and useful qualitative information on the seismic performance and financial implications of URM houses, the dollar values obtained are only representative and are not precise because of the assumptions and approximations that have been made in the process. Although variations in the capacity and demand and the modelling uncertainty have been quantitatively incorporated in the form of corresponding lognormal coefficients of variation, uncertainties in the assumed loss model have not been accounted for. The values assigned in this study to loss ratios and drift ratios for different damage states are also somewhat subjective. EAL is sensitive to the loss ratio corresponding to different damage states; especially those for DS2

and DS3. Hence, future studies should try to establish more robust damage model and loss model and investigate their uncertainties so that they could be accounted for in estimating the financial risk.

## 9. References


1. Arya, A. S., (1992). *Masonry and Timber Structures including Earthquake Resistant* Design, Nem Chand & Bros., Roorkee, India.
2. ATC, (1996). *ATC 40 Seismic Evaluation and Retrofit of Concrete Buildings*, Vol. 1, Applied Technology Council, California, USA.
3. Benedetti, D. and Pezzoli, P., (1996). *Shaking Table Test on Masonry Buildings: Results and Comments*, ISMES S. p. a., via Pastrengo, 24068 Seriate – Bergamo, Italy.
4. Bothara, J. K., (2004). *A shaking table investigation on the seismic resistance of a brick masonry house*, Masters' Thesis, University of Canterbury, Christchurch, New Zealand.
5. Bracci, J. M., Reinhorn, A. M. and Mander, J. B., (1992). *Seismic Resistance of Reinforced Concrete Frame Structures Designed only for Gravity, Part I: Design and Properties of One-third Scale Model Structure*, Technical Report NCEER-92-0027.
6. Bruneau, M., (1994). *State-of-the-Art Report on Seismic Performance of Unreinforced Masonry Buildings*, J. of Structural Engineering, Vol. 120, No. 1, ASCE, pp 230-251.
7. Calvi, G. M., and Pavese, A., (1995). *Application of dynamic Identification Techniques to a Brick Masonry Building Prototype*, Proceedings of 10th European Conference on Earthquake Engineering, Vol. 3, pp 2413-2418.
8. Chopra, A. K., (1995). *Dynamics of Structures*, Prentice- Hall of India Private Limited, New Delhi.
9. Costley, A. C., and Abrams, S. P., (1996). *Dynamic Response of Unreinforced Masonry Buildings with Flexible Diaphragm*, Technical Report NCEER-96-0001.
10. Craig, J.I., Goodno, B.J., Towashiraporn, P., Park, J., 2002, "Fragility Reduction Estimations for URM Buildings Using Response Modification," Proceedings, 12th European Conference on Earthquake Engineering Research, Paper No. 805, London, September 9 - 13.
11. De Felice, G. and Giannini, R., (2000). *Assessment of Vulnerability to Out-of-plane Collapse of Masonry Walls*, Proceedings of World Conference on Earthquake Engineering, Paper No. 0715, Auckland, New Zealand.
12. De Felice, G. and Giannini, R., (2001). *Out-of-plane Seismic Resistance of Masonry Walls*, J. of Earthquake Engineering, Vol. 5, No. 2, pp 253-271.
13. Dhakal, R. P. and Mander, J. B. 2005. Probabilistic Risk Assessment Methodology Framework for Natural Hazards, Report submitted to Institute of Geological and Nuclear Science (IGNS), Department of Civil Engineering, University of Canterbury, Christchurch, New Zealand.
14. Dhanasekar, M., Page, A. W., and Kleeman, P. W., (1982). *The Elastic Properties of Brick Masonry*, International J. of Masonry Construction, Vol. 2, pp 155-160.
15. Doherty, K. T., (2000). *An Investigation of the Weaklinks in the Seismic Load Path of Unreinforced Masonry Buildings*, Ph.D. Thesis, Faculty of Engineering, University of Adelaid, Australia.
16. Doherty, K. T., Griffith, M. C., Lam, N., and Wilson, J., (2002). *Displacement-based Seismic Analysis for the Out-of-plane Bending of Unreinforced Masonry Walls*, Earthquake Engineering and Structural Dynamics, Vol. 31, pp 833-850.
17. FEMA, (1978). *FEMA 154 Rapid Visual Screening of Buildings with Potential Seismic Hazard: A Handbook*, Federal Emergency Management Agency, Washington, DC, USA.

18. FEMA, (2000). *FEMA 356 Prestandard and Commentary for the Seismic Rehabilitation of Buildings*, Federal Emergency Management Agency, Washington, DC, USA.

19. Griffith, M. C. and Magenes, G., (2003). *Accuracy of Displacement based Evaluation of URM Wall Stability*, Proceedings of Pacific Conference on Earthquake Engineering, Paper No. 127, Christchurch, New Zealand.

20. Griffith, M. C., Magenes, G., Melis, G. and Picchi, L., (2003). *Evaluation of Out-of-plane Stability of Unreinforced Masonry Walslsubjected to seismic excitation*, J. of Earthquake Engineering, Vol. 7, Special Issue 1, pp 141-169.

21. HAZUS. 1999, *Earthquake Loss Estimation Methodology.* Technical Manual. Prepared by the National Institute of Building Sciences for Federal Emergency Management Agency, Washington, DC.

22. Kennedy, R.P, Cornell, C.A, Campbell R.D, Kaplan, S and Perla H.F, 1980, *Probabilistic Seismic Safety Study of an Existing Nuclear Power Plant*, Nuclear Engineering and Design No. 59, pp 315-338.

23. Krawinkler H. and Miranda E., 2004, *Performance-Based Earthquake Engineering*, Earthquake Engineering: From Engineering Seismology to Performance-Based Engineering, edited by Bozorgnia Y. and Bertero V.V. CRC Press, Boca Raton, FL.

24. Magenes, G., (2000). *A method for pushover analysis in seismic assessment of masonry buildings*, 12th World Conference on Earthquake Engineering, Auckland, New Zealand (CD-ROM).

25. Magenes, G. and Calvi, G. M., (1995). *Shaking Table Tests on Brick Masonry Walls*, Proceedings of 10th European Conference on Earthquake Engineering, Vol. 3, pp 2419-2424.

26. Magenes, G. and Calvi, G. M., (1997). *In-plane Seismic response of Brick Masonry Walls*, Earthquake Engineering and Structural Dynamics, Vol. 26, pp 1091-1112.

27. Mahanay, J. A., Paret, T. F., Kehoe, B. E. and Freeman, S. A., (1993). *The Capacity Spectrum Method for Evaluating Spectral Response During Loma Prieta Earthquake*, National Earthquake Conference, Memphis, USA (Referred in ATC 40).

28. Martinez, M. E., (2002). *Performance-based Seismic Design and Probabilistic Assessment of Reinforced Concrete Moment Resisting Frame Structures*, Masters' Thesis, University of Canterbury, Christchurch, New Zealand.

29. Mengi, Y. and McNiven, H. D., (1986). *A Mathematical Model for Predicting the Non-linear Response of Unreinforced Masonry Walls to In-plane Earthquake Excitation*, Earthquake Engineering Research Centre, Report No. UCB/EERC-86/07, Berkeley, USA.

30. Moon FL, Yi TY, Leon RT, et al. (2006). Recommendations for seismic evaluation and retrofit of low-rise URM structures. Journal of Structural Engineering-ASCE 132 (5): 663-672.

31. NSET, (1999). *Reconnaissance Report on Chamoli Earthquake of 29 March 1999, India*; (http://www.adpc.net/audmp/projectoutputs/nepal/report-chamoli-eq-1.pdf) A joint study report by National Society for Earthquake Technology-Nepal, and Department of Earthquake Engineering, University of Roorkee.

32. NSET, (2000). *Seismic Vulnerability of School Buildings of Kathmandu Valley and Methods for Reducing it (Unpublished)*, The Kathmandu Valley Earthquake Risk Management Project implemented by National Society for Earthquake Technology Kathmandu, Nepal.

33. NZS 1170.5:2004 Part 5: Structural Design Actions, Earthquake Actions-New Zealand. Standard Association of New Zealand, Wellington.

34. NZS3101:1995, Standards New Zealand, 1995, Concrete Structures Standard, NZS 3101, Parts 1 & 2, Standards New Zealand.

35. NZSEE, 2006, Assessment and Improvement of the Structural Performance of Buildings in Earthquake, New Zealand Society for Earthquake Engineering, Wellington, NZ.

36. NZSEE, (1995). *Draft Guidelines for Assessing and Strengthening Earthquake risk Buildings*, New Zealand Society of Earthquake Engineering, Wellington, NZ.

37. Park, J., Craig, J.I., Goodno, B.J., 2002, "Simple nonlinear in-plane response models for assessing fragility of URM walls," 7NCEE, Boston, MA, July 21-25.

38. Paulay, T. and Priestley, M. J. N., (1992). *Seismic Design of Reinforced Concrete and Masonry Buildings*, John Wiley & Sons Inc. NY, USA.

39. Pekcan, G., Mander, J. B. and Chen, S. S., (1999), Fundamental Considerations for the Design of Non-linear Viscous Dampers, Earthquake Engineering and Structural Dynamics, Vol. 28, pp 1405-1425.

40. Peralta, D.F., Hueste, M.B.D., Bracci, J.M., 2002, "Seismic performance of rehabilitated floor and roof diaphragms in pre-1950s unreinforced masonry buildings," 7NCEE, Boston, MA, July 21-25.

41. Priestley, M. J. N., 1985, *Seismic Behaviour of Unreinforced Masonry Walls*, Bulletin of the New Zealand Society for Earthquake Engineering, Vol. 18, no 2, pp 191-205.

42. Qamaruddin, M. and Chandra, B., (1991). *Behaviour of Unreinforced Masonry Buildings subjected to Earthquakes*, Professional J. of Masonry Society, Vol. 9, No. 12, pp 47-55, The Masonry Society, USA.

43. SAP2000, (2002). *Integrated Software for Structural Analysis and Design*, Computer and Structures, Inc. Berkeley, California, USA.

44. Simsir, C., Aschheim, M., and Abrams, D., 2002, "Influence of diaphragm flexibility on the out-of-plane response of unreinforced masonry bearing walls," 9th North American Masonry Conference, Clemson, South Carolina, June 1-4.

45. Sobaih, M., (1999). *Seismic Hazard and Counter Measures in Giza City*, Bulletin of International Institute of Seismology and Earthquake Engineering, Vol. 33, Building Research Institute, Tsukuba, Japan.

46. Tena-Colunga A, Abrams D. (1992). Response of an unreinforced masonry building during the Loma Prieta Earthquake. Structure Research, No. 576, Department of Civil Engineering, University of Illinois at Urbana-Champaign, IL.

47. Tomazevic, M., (1987). *Dynamic Modelling of Masonry Buildings: Storey Mechanism as a Simple Alternative*, Earthquake Engineering and Structural Dynamics, Vol. 15, No. 6, pp 731-749.

48. Tomazevic, M., (1996). *Seismic Upgrading of old Brick-Masonry Urban Houses: Tying of Walls with Steel Ties*, Earthquake Spectra, Vol. 12, No. 3, pp 599-622.

49. Tomazovic, M., 1999, *Earthquake Resistant Design of Masonry Buildings,* ISBN 1-86094-066-8, Imperial College Press.

50. Towashiraporn, P., Park, J., Craig, J.I., Goodno, B.J., 2002, "Fragility reduction for URM building using passive response modification," 7NCEE, Boston, MA, July 21-25.

51. Yi TY, Moon FL, Leon RT, et al. (2006a). Lateral load tests on a two-story unreinforced masonry building. Journal of Structural Engineering-ASCE 132 (5): 643-652.

52. Yi TY, Moon FL, Leon RT, et al. (2006b). Analyses of a two-story unreinforced masonry building. Journal of Structural Engineering -ASCE 132 (5): 653-662.

Table 1 Material properties

| **Material** | **Test type** | **Test result** | **CoV** | **Remarks** |
|---|---|---|---|---|
| Brick | Compressive | 26.6 MPa | 17% | |
| | Initial rate of absorption (IRA) | 63.6 gram | 7.4% | |
| Mortar Cubes | Compressive | 7.6 MPa | 10.6% | |
| Masonry Prism | Compressive | 16.2 MPa | 19.7% | At strain 0.0035 |
| | Young's Modulus, E | 6100 MPa | 45.2% | At strain 0.0016 |
| | Shear Strength | $\tau_o$ =0.93 MPa | 38.6% | |
| | | $\phi$ = 44.4º | 13.4% | |
| | Flexural Bond | 0.42 MPa | 35% | |
| | Split Bond | 0.41 MPa | 38% | |

Table 2 Longitudinal shaking test sequence

| S. No. | Acceleration Record | PGA (g) | Code | Purpose |
|---|---|---|---|---|
| 1 | White noise | 0.02g | Wn (0.02) | Study of dynamic characteristics |
| 2 | White noise | 0.05g | Wn (0.05) | Study of dynamic characteristics |
| 3 | Taft2721 | 0.2g | Taft (0.2) | Moderate level earthquake |
| 4 | Taft2721 | 0.3g | Taft (0.3) | Moderate level earthquake |
| 5 | Umbria March (RA01168 551) | 0.5g | Ra01168 551 (0.5g) | Severe earthquake |
| 6 | El-Centro | 0.348g | EL40NSC | Moderate to severe earthquake |

Table 3 Transverse shaking test sequence

| S. No. | Acceleration Record | PGA (g) | Code | Purpose |
|---|---|---|---|---|
| 1 | White noise | 0.05g | Wn (0.05) | Study of dynamic characteristics |
| 2 | Taft2721 | 0.2g | Taft (0.2) | Moderate level earthquake |
| 3 | White noise | 0.05g | Wn (0.05) | Study of dynamic characteristics |
| 4 | Taft2721 | 0.3g | Taft (0.3) | Moderate level earthquake |
| 5 | White noise | 0.05g | Wn (0.05) | Study of dynamic characteristics |
| 6 | White noise | 0.05g | Wn (0.05) | Study of dynamic characteristics |
| 7 | El-Centro | 0.348g | EL40NSC | Moderate level earthquake |
| 8 | White noise | 0.05g | Wn (0.05) | Study of dynamic characteristics |
| 9 | Umbria March (RA01168 551) | 0.5g | Ra01168 551 (0.5g) | Severe earthquake |
| 10 | Umbria March (RA01168 551) | 0.7g | Ra01168 551 (0.7g) | Severe earthquake |
| 11 | White noise | 0.05g | Wn (0.05) | Study of dynamic characteristics |
| 12 | North Ridge | 0.8g | Sylm949 | Strong earthquake |
| 13 | Nahanni | 0.8g | Nahanni | Strong earthquake |
| 14 | White noise | 0.05g | Wn (0.05) | Study of dynamic characteristics |

Table 4 Maximum displacements at the seismic mass centre and measured hysteretic damping

| Shaking Direction | Excitation | Maximum displacement | Measured hysteretic damping (%) |
|---|---|---|---|
| Longitudinal | Taft (0.2) | 0.98 | 9.1 |
| | Taft (0.3) | 0.82 | 7.3 |
| | Ra01168 551(0.5g) | 3.9 | 31.5 |
| | EL40NSC | 2.36 | 18.5 |
| Transverse | Taft (0.2) | 2.58 | 15.9 |
| | Taft (0.3) | 3.74 | 22.6 |
| | EL40NSC | 4.65 | 21.5 |
| | Ra01168 551(0.5g) | 6.85 | 39.4 |
| | Ra01168 551(0.7g) | 10.07 | 41.9 |
| | Sylm949 | 11.1 | 52.3 |
| | Nahanni | 15.33 | 30.3 |

Table 5 Estimated lateral load coefficient for initiation of cracking and corresponding deflections

| Loading direction | Base shear coefficient at crack initiation | Deflections | | | | | | | | Remarks |
|---|---|---|---|---|---|---|---|---|---|---|
| | | In-plane wall-1 | | In plane wall-2 | | Out-of-plane-1 | | Displacement of seismic mass | | |
| | | 1st Floor | Eaves level | 1st Floor | Eaves level | 1st Floor | Eaves level | 1st Floor | Eaves level | |
| Longitudinal | 0.36 | 0.89 | 1.3 | 1.03 | 1.63 | 0.92 | 1.49 | 0.94 | 1.47 | Controlled by in-plane cracking |
| Transverse | 0.30 | 0.77 | 1.6 | 0.65 | 1.45 | 0.8 | 1.99 | 0.79 | 1.85 | Controlled by out-of-plane cracking |

Table 6 Dynamic characteristics of model

| Shaking Direction | Method of Analysis | Frequencies (Hz) | | Mode shapes | |
|---|---|---|---|---|---|
| | | Analytical | Experimental | Analytical | Experimental |
| Longitudinal | Static Condensation | $\begin{Bmatrix}10\\28\end{Bmatrix}$ | (11.7) | $\begin{bmatrix}1.0 & -0.77\\0.72 & 1.0\end{bmatrix}$ | $\begin{Bmatrix}1\\0.81\end{Bmatrix}$ |
| | FEM-SAP2000 | (8.7) | | | |
| Transverse | Static Condensation | $\begin{Bmatrix}9.3\\21.7\end{Bmatrix}$ | (9.8) | $\begin{bmatrix}1.0 & -0.72\\0.55 & 1.0\end{bmatrix}$ | $\begin{Bmatrix}1\\0.49\end{Bmatrix}$ |
| | FEM-SAP2000 | (7.5) | | | |

Table 7 HAZUS classification of damage states following an earthquake (HAZUS, 1999)

| Damage State | Damage Descriptor | Post-earthquake Utility of Structure |
|---|---|---|
| 1 | None (pre-yield) | Normal |
| 2 | Minor / Slight | Slight Damage |
| 3 | Moderate | Repairable Damage |
| 4 | Major / Extensive | Irreparable Damage |
| 5 | Complete Collapse | |

Table 8 Damage state classification

| Damage State | Drift Limits (%) | $\Delta_{experimental}$ (mm) | $\zeta_{effective}$ (%) | $B_\zeta$ | $\Delta_{prototype}$ (mm) | Expected PGA | Post earthquake utility |
|---|---|---|---|---|---|---|---|
| 1 | | | | | | | No Damage |
| | 0.1 | 2 | 20.1 | 1.58 | 4 | 0.35 | |
| 2 | | | | | | | Slight Damage |
| | 0.5 | 10 | 33.5 | 1.96 | 20 | 0.43 | |
| 3 | | | | | | | Repairable Damage |
| | 0.9 | 18 | 35.0 | 2.0 | 36 | 0.56 | |
| 4 | | | | | | | Irreparable Damage |
| | 1.3 | 26 | 35.5 | 2.01 | 52 | 0.68 | |
| 5 | | | | | | | Complete Collapse |

Table 9 Probability of not exceeding different damage states (P[DS ≤ DSi]) of an URM house

| $f_a$ | i=1 | i=2 | i=3 | i=4 | i=5 |
|---|---|---|---|---|---|
| 0.1 | 0.97 | 1 | 1 | 1 | 1 |
| 0.01 | 0.74 | 0.84 | 0.92 | 0.96 | 1 |
| 0.001 | 0.26 | 0.39 | 0.56 | 0.69 | 1 |
| 0.0001 | 0.03 | 0.06 | 0.12 | 0.22 | 1 |
| 0.00001 | 0 | 0 | 0.02 | 0.02 | 1 |
| 0.000001 | 0 | 0 | 0 | 0 | 1 |

Table 10 Probability of being in a given damage state; i.e. confidence interval (P[DS = DSi]) of an URM house

| $f_a$ | i=1 | i=2 | i=3 | i=4 | i=5 |
|---|---|---|---|---|---|
| 0.1 | 0.97 | 0.03 | 0 | 0 | 0 |
| 0.01 | 0.74 | 0.1 | 0.08 | 0.04 | 0.04 |
| 0.001 | 0.26 | 0.13 | 0.17 | 0.13 | 0.31 |
| 0.0001 | 0.03 | 0.03 | 0.06 | 0.1 | 0.78 |
| 0.00001 | 0 | 0 | 0.02 | 0 | 0.98 |
| 0.000001 | 0 | 0 | 0 | 0 | 1 |

Table 11 Loss ratios for different damage states

| | DS1 | DS2 | DS3 | DS4 | DS5 |
|---|---|---|---|---|---|
| Likely Range | 0 | 0.05-0.15 | 0.2-0.4 | 1.0-1.2 | 1 |
| Assumed $L_R$ value | 0 | 0.1 | 0.3 | 1 | 1 |

Table 12 Probable loss contributed by different damage states

| $f_a$ | $L_R$[DS1] | $L_R$[DS2] | $L_R$[DS3] | $L_R$[DS4] | $L_R$[DS5] | Total $L_R$ |
|---|---|---|---|---|---|---|
| 0.1 | 0 | 0.003 | 0 | 0 | 0 | 0.003 |
| 0.01 | 0 | 0.01 | 0.024 | 0.04 | 0.04 | 0.114 |
| 0.001 | 0 | 0.013 | 0.051 | 0.13 | 0.31 | 0.504 |
| 0.0001 | 0 | 0.003 | 0.018 | 0.1 | 0.78 | 0.901 |
| 0.00001 | 0 | 0 | 0.006 | 0 | 0.98 | 0.986 |
| 0.000001 | 0 | 0 | 0 | 0 | 1 | 1 |

Table 13 Annual financial risk for typical URM houses

| | EAL (per $1 million) | |
|---|---|---|
| | $L_R$ | ΔEAL |
| 0.1 | 0.003 | |
| | | 5265 |
| 0.01 | 0.0114 | |
| | | 2781 |
| 0.001 | 0.504 | |
| | | 632 |
| 0.0001 | 0.901 | |
| | | 85 |
| 0.00001 | 0.986 | |
| | | 9 |
| 0.000001 | 1 | |
| Total EAL per $1million | | 8772 |

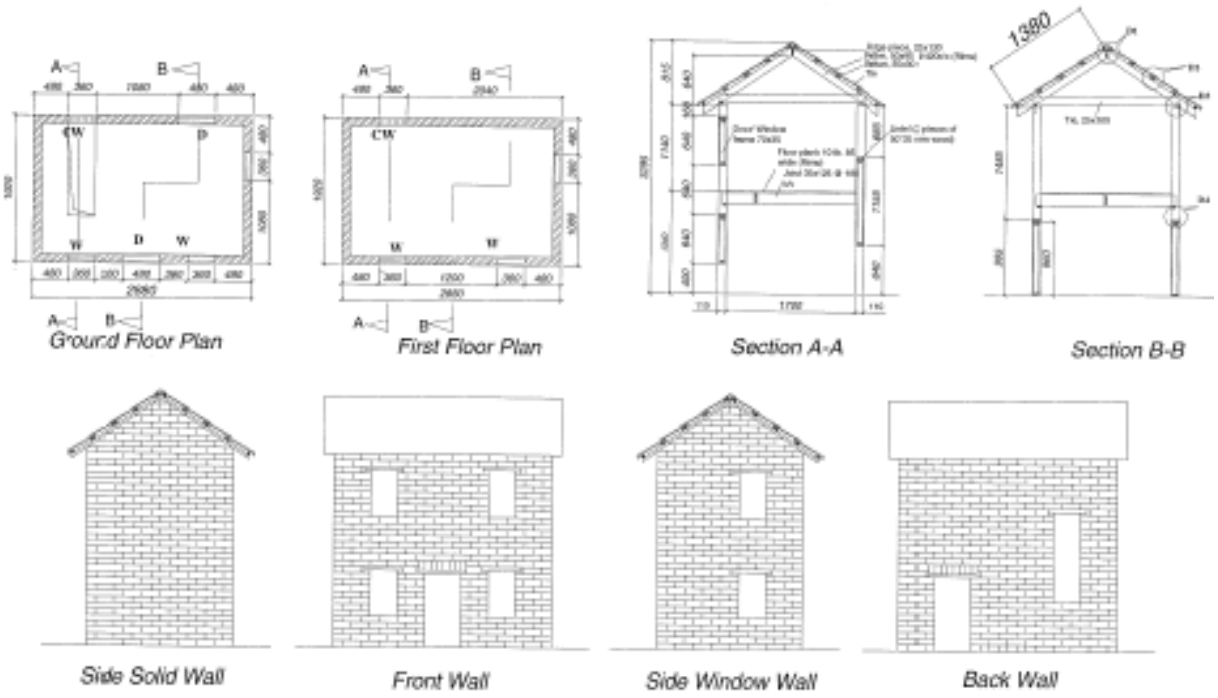


**Figure 1** Plan and elevation of the model

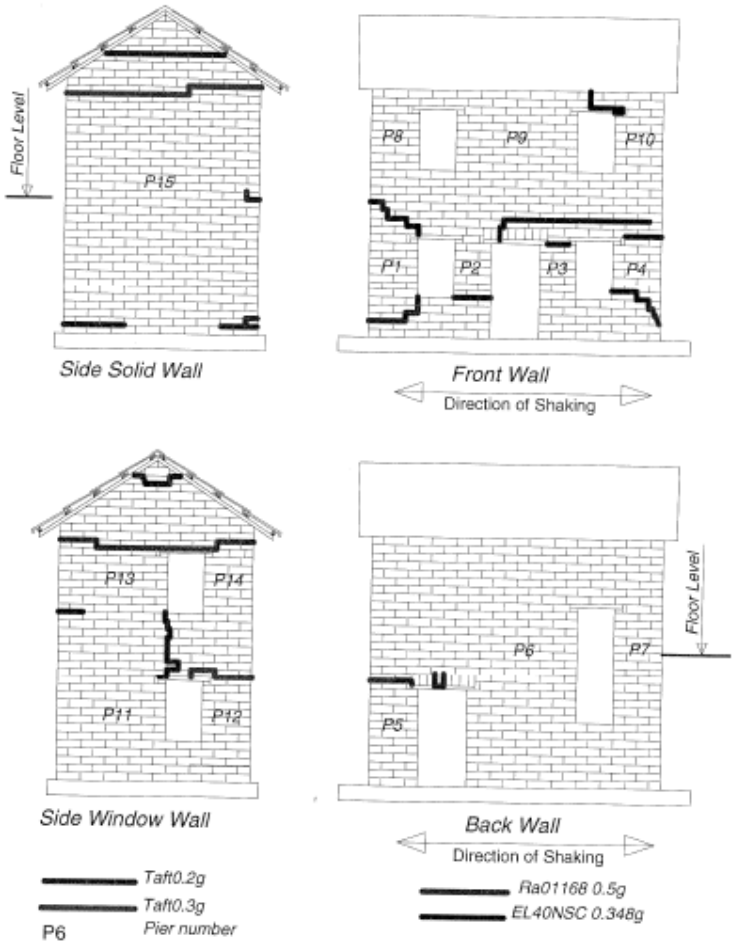


**Figure 2** Crack propagation pattern and their locations (longitudinal direction)

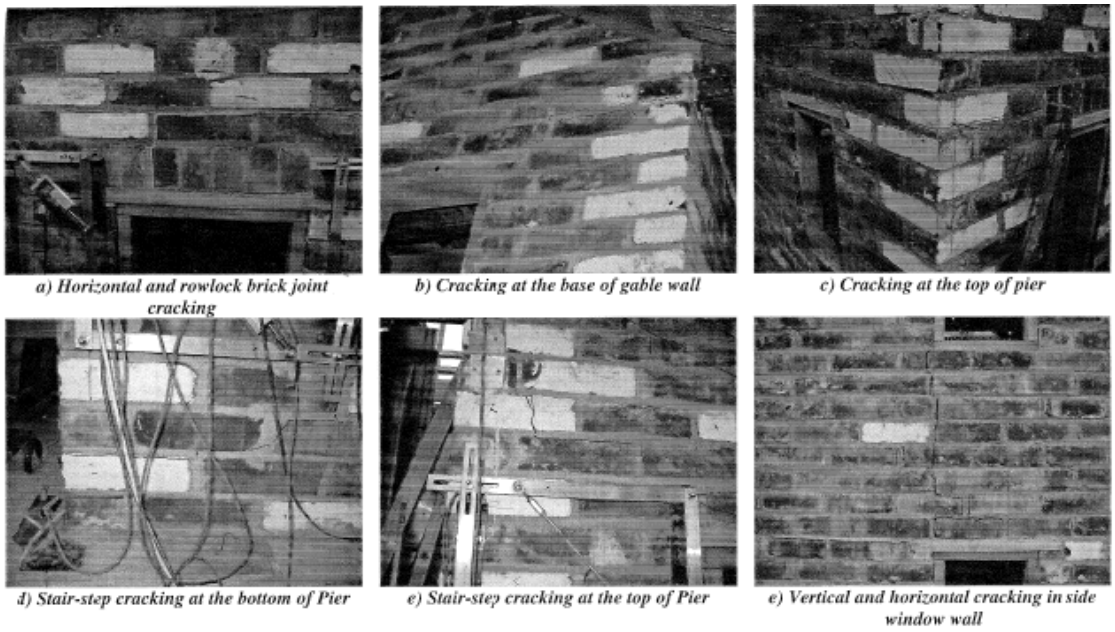


**Figure 3** Visually observed damage during excitation (longitudinal direction)

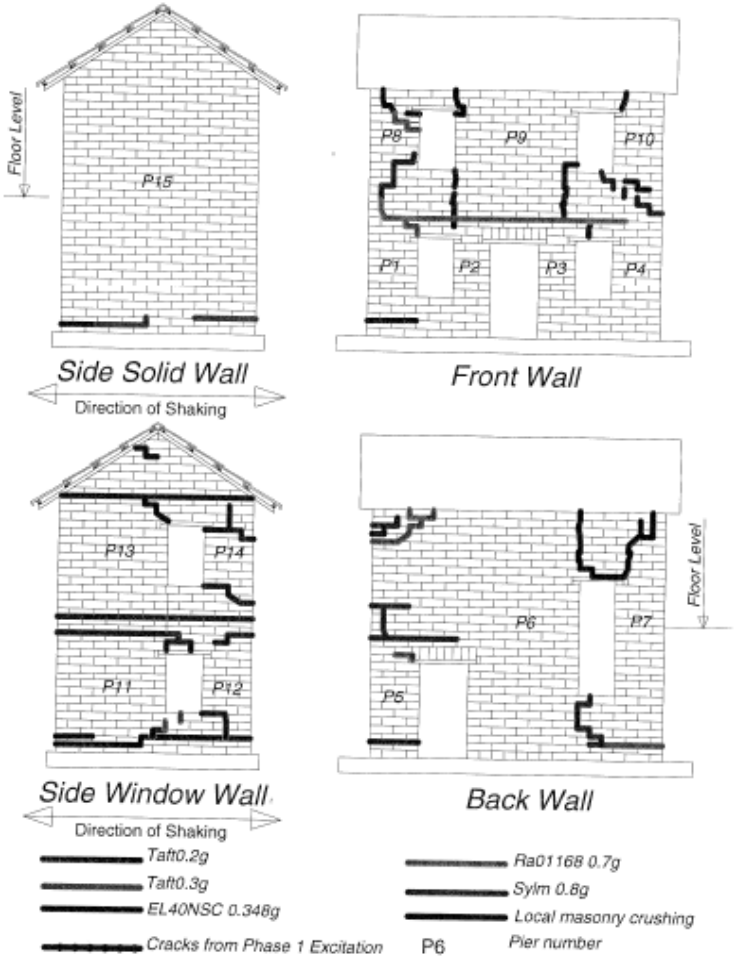


**Figure 4** Crack propagation pattern and their locations (Transverse direction)

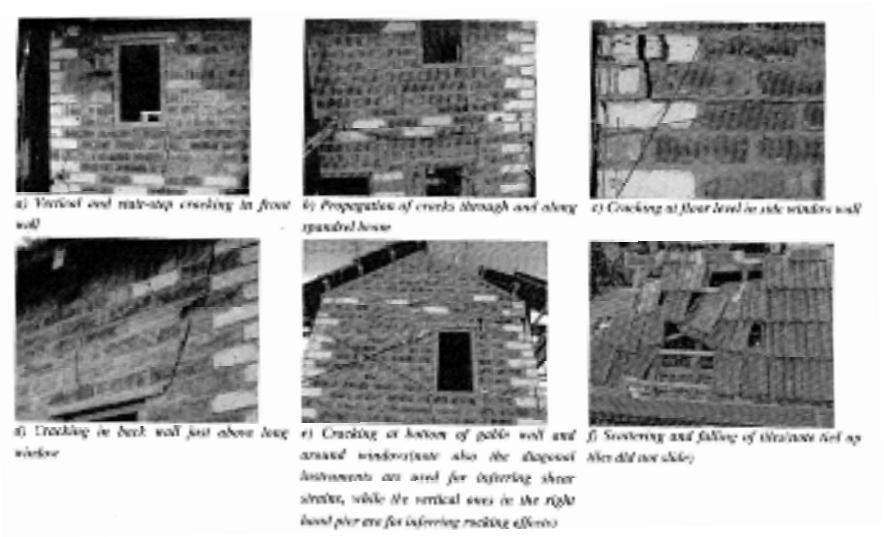


**Figure 5** Visually observed damage during excitation (Transverse direction)

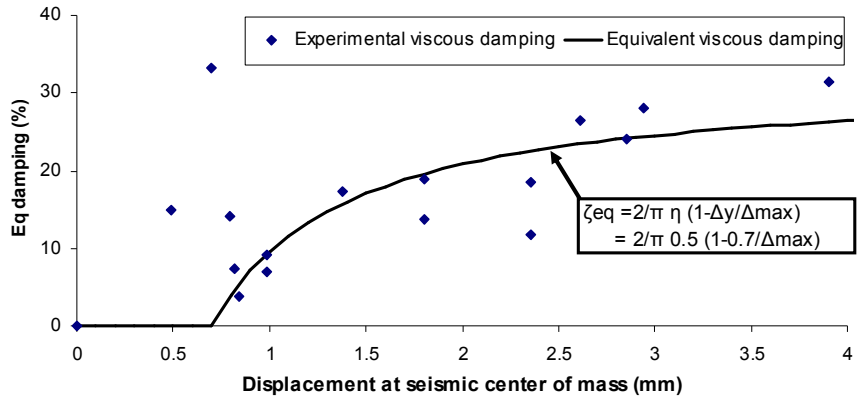


*a) Longitudinal shaking*

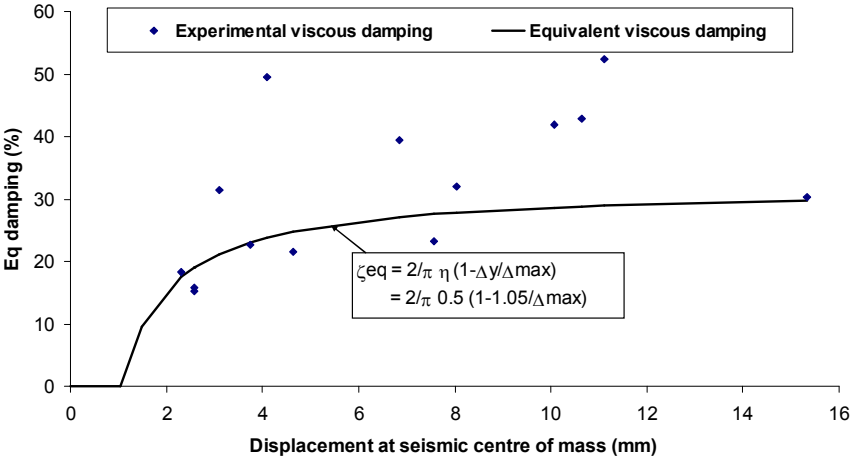


*b) Transverse shaking*

**Figure 6** Theoretical prediction and experimental verification of displacement versus equivalent viscous damping representative of hysteretic response (a) longitudinal direction; (b) transverse direction

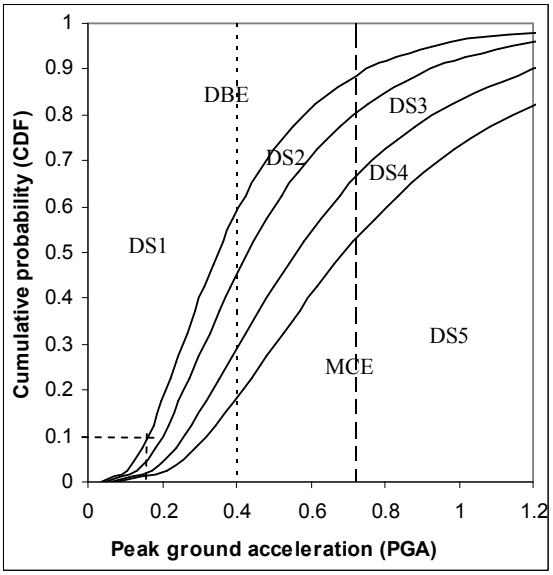


**Figure 7** Vulnerability curves related to the HAZUS damage states.

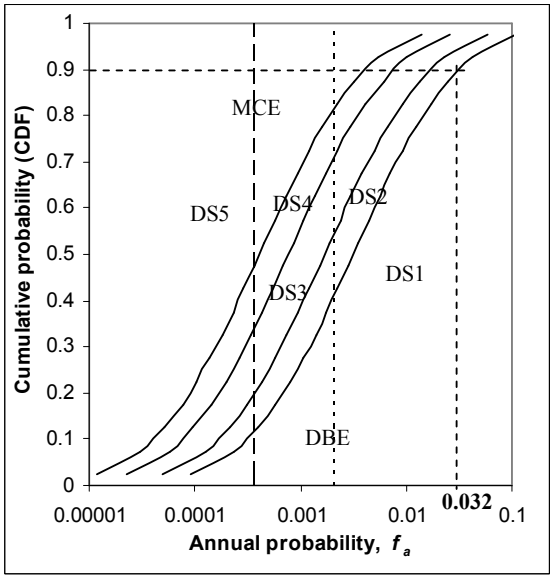


**Figure 8** Hazard survival curves related to the HAZUS damage states.

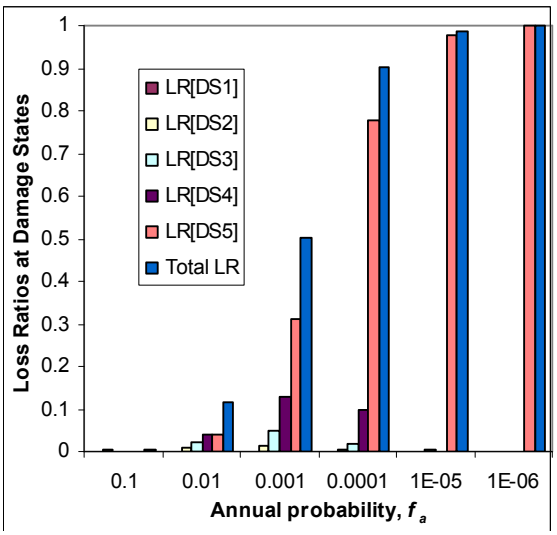


**Figure 9** Deaggregation of loss contributed by different damage states.

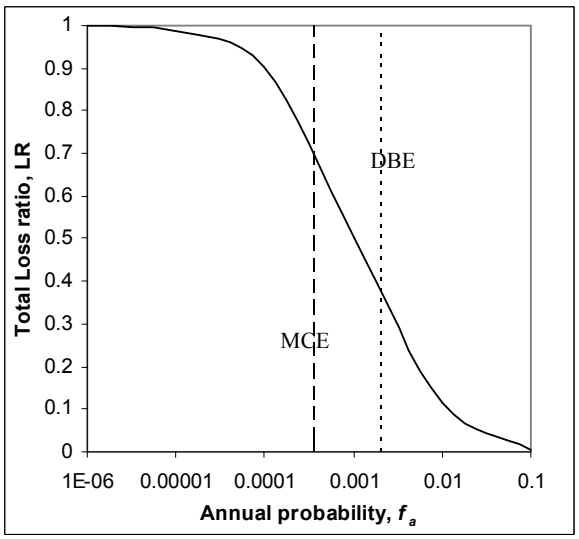


**Figure 10** Loss hazard curve

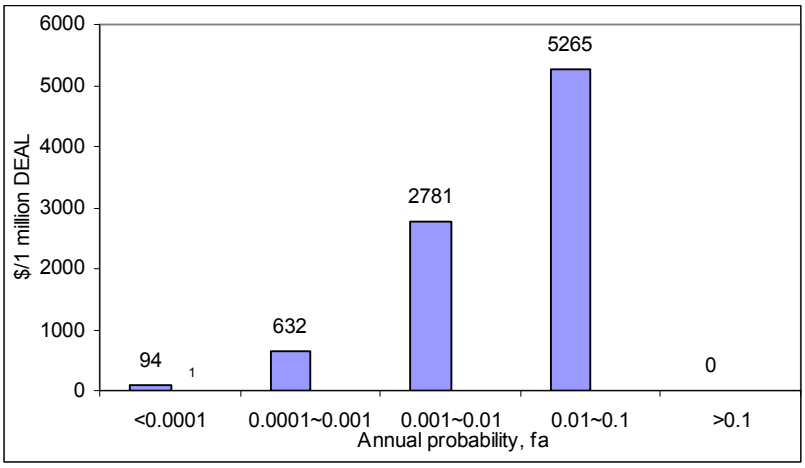


**Figure 11** Annual financial risk due to earthquakes of different frequency ranges